



NLR-TP-2004-409

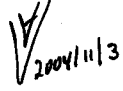
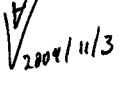
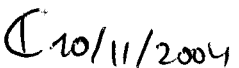
A framework for aeroelastic simulations of trimmed rotor systems in forward flight

H. van der Ven and O.J. Boelens

The work described in this report is partially funded by the EU 6FP
'FRIENDCOPTER' project under contract no. AIP3-CT-2003-502773, and partially
by NLR's basic research programme.

No part of this report may be reproduced and/or disclosed, in any form or by any
means without the prior written permission of the owner.

Customer: National Aerospace Laboratory NLR
Working Plan number: AV.1.B.4
Owner: National Aerospace Laboratory NLR
Division: Aerospace Vehicles
Distribution: Unlimited
Classification title: Unclassified
October 2004

Approved by author: 	Approved by project manager: 	Approved by project managing department: 
--	---	--



Contents

Summary	3
1 Introduction	5
1.1 Vibrational analysis	5
1.2 A classification of analysis methods	6
1.3 Towards advanced rotor codes	8
1.4 Outline	9
2 Multitime multigrid algorithm	10
2.1 Basic idea	10
2.2 Benefits	10
3 Rotorcraft simulation	13
3.1 Structural model	13
3.2 Aerodynamic model	14
3.3 Flight conditions	14
3.4 Trim	15
3.5 Grid adaptation	15
3.6 Simulation strategy	16
3.7 Results	16
3.7.1 Trim	16
3.7.2 Temporal adaptation	16
3.7.3 Space-time adaptation	19
3.7.4 Final trim	20
3.8 Computational complexity	20
4 Conclusions	27
5 References	28

3 Tables

12 Figures

(29 pages in total)

Summary

Heavy vibratory loading of rotorcraft is relevant for many operational aspects of helicopters, such as the structural life span of (rotating) components, operational availability, the pilot's comfort, and the effectiveness of weapon targeting systems. A precise understanding of the source of these vibrational loads has important consequences in these application areas. Near the border of the flight envelope current analysis tools can be improved with respect to the level of physical modeling of the flow phenomena which contribute to the vibratory loads. The required first-principles-based analysis tools, however, display prohibitively large computing times when applied in a straightforward way. In this paper a revolutionary solution approach is applied to the simulation of the trimmed, aeroelastic, BO105 rotor system in forward flight. The simulation will demonstrate that the relevant physical phenomena are captured, and that the solution approach renders the application of first-principle-based aerodynamics tools feasible for the prediction of vibratory loads for rotorcraft.



Symbols and abbreviations

a_∞	freestream speed of sound
BVI	Blade-Vortex Interaction
CFD	Computational Fluid Dynamics
C_T	thrust coefficient
C_{M_x}	roll moment coefficient
C_{M_y}	pitch moment coefficient
HUM	Health and Usage Monitoring
L	sectional lift coefficient normalised by $m_{\text{ref}}R\Omega^2$
M	sectional moment coefficient normalised by $m_{\text{ref}}R^2\Omega^2$
MTMG	Multitime Multigrid algorithm
m_{ref}	blade mass
Ω	blade passing frequency
Ψ	azimuth angle
r	spanwise blade station
R	blade radius
θ	elastic pitch
θ_{con}	pitch schedule
θ_0	collective pitch
θ_{1c}	longitudinal pitch
θ_{1s}	lateral pitch
w	elastic bending
ξ	computational beam coordinate



1 Introduction

1.1 Vibrational analysis

In his address to the House Armed Services Committee, March 2004, M.E. Rhett Flater, executive director of the American Helicopter Society International, defended the need for a helicopter industrial base by stating: “Because of their complexity, high vibration, and heavy loading, helicopters are maintenance-intensive vehicles, requiring constant support in the field in order to assure high combat availability. In addition, many combat environments require that the fleet undergo emergency upgrades to address adverse local conditions, such as Afghanistan’s hot-high environment or the sandstorms of Iraq, (. . .).” As cited, the high vibrational loading is an important contributor to the maintenance issues of rotorcraft and affects its operational availability. A precise understanding of the sources of these vibrational loads has important consequences in the following application area’s:

Safety and costs. In recent years, life cycle management and the installation of Health and Usage Monitoring (HUM) Systems onboard rotorcraft has resulted in higher operational safety levels. A HUM System can be used to notify a problem during or after a mission, resulting in mission abort and/or in a costly grounding of the aircraft. Usage monitoring systems are generally not based on a physical understanding of the sources of the vibrational loads and use statistical or genetic methods to identify possible component failures or fault conditions (Haas et al.8, Stevens et al.19). Combination of a HUM system and a physics-based capability to predict the loads will increase the diagnostic and prognostic capability of the HUM system whilst including a physical understanding of the sources of the vibrational loads as well as the history of these loads for the specific aircraft. Moreover, the predictive capability can be used to perform a model-based diagnosis of the vibratory signals to improve the component-loads-monitoring capability of the HUM system (Stevens et al.19), decrease the number of false alarms (Tumer et al.20, 21), and improve the flight-regime-detection capability (McCool et al.14).

Comfort. Long exposure to vibrational loads is an important cause of negative moods and increased back pain (Gander et al.7) in the crew of the helicopter.

Weapon targeting. As mentioned by Tom Curtis, program manager of the U.S. Marine attack and utility helicopters, in the National Defense Magazine, July 2001, the night targeting system of the Cobra helicopter “bounces around”, since the system’s sensor is smeared by vibration. A reduction of vibration levels would clearly improve the helicopter’s targeting effectiveness.

level	model
1	linear beam model for blade, no hub/pylon model
2	nonlinear beam model, simple hub/pylon model
3	multi-body dynamics model blade/hub/pylon

Table 1 The different sophistication levels in the modeling of the structural dynamics of helicopters.

level	model
1	lifting line or lookup tables, fixed wake vortex model
2	full-potential flow near blade, free-wake vortex model
3	CFD (Euler/Navier-Stokes)

Table 2 The different sophistication levels in the modeling of the aerodynamics of helicopters.

1.2 A classification of analysis methods

Several analysis methods for helicopters are available at different levels of sophistication in the representation of the physical phenomena associated with vibrational analysis. For helicopters, these phenomena are described by structural dynamics, aerodynamics, and flight control, which are tightly coupled. Table 1, resp. 2, tabulate the different sophistication levels in the modeling of the structural, resp. aerodynamics, of helicopters.

Based on this classification three levels of helicopter dynamics modeling can be determined:

A. Comprehensive rotor codes

Comprehensive rotor codes such as CAMRAD/JA and FlightLab have sophistication level 2 for the structural dynamics and sophistication level 1 for the aerodynamics. The low level aerodynamics modeling results in an efficient analysis tool for the performance of helicopters. The higher harmonics of the aerodynamic loads are, however, less well predicted, resulting in a less than optimal prediction of the blade motion (even though the structural dynamics is well represented).

The importance of the accurate prediction of the blade motions under aerodynamic and structural loading has been stressed by, among others, Burley et al. 4 in the context of the TRAC program.

The blade loads, and hence the vibrational loads on the fuselage, are extremely sensitive to the elastic motions of the blades. As found by Milgram et al. 15 and Yeo et al. 26, comprehensive rotor codes are not capable to supply the higher harmonics of the blade loads which are needed for vibrational analysis, even for isolated rotors. Lyle et al. 13 were surprised of the good correlation between experiment and simulation for the lower harmonics, and cautioned against extrapolation of the results to other flight conditions.

B. Higher level rotor codes

In order to resolve the inadequacies of the comprehensive rotor codes, rotor codes have been developed with improved aerodynamical modeling, based on full-potential flow near the blades, and a free-wake vortex model in the wake (Hounjet et al.9). Such codes have sophistication level 2 for the structural dynamics and sophistication level 2 for the aerodynamics. The improved accuracy in the prediction of the aerodynamic loads results in a more accurate prediction of the blade motions, making these codes suitable for vibrational analysis for flight conditions in the interior of the flight envelope. The aerodynamics model, however, is not able to represent important flow phenomena, such as Blade Vortex Interaction (BVI), stall, etc., which occur near the border of the flight envelope.

C. Advanced rotor codes

In order to be able to represent the flow phenomena near the border of the flight envelope, aerodynamic models based on first-principles flow physics are required, at sophistication level 3. Such models constitute an important step into representing BVI, High Speed Impulsive (HSI) effects, dynamic stall, buffeting, and twin vortices occurring at tilt rotor flow in certain hover conditions.

As shown by Boelens et al. 3 through the simulation of the flow about the rigid blades of the Operational Loads Survey rotor in forward flight, aerodynamic tools based on first principles of flow physics are capable of capturing BVI events which can be identified as a cause for vibratory loads.

Conventional models of this type display a significantly higher computational complexity (as will be discussed in the next section), and may therefore be coupled with advanced structural models of the rotor/hub/pylon system without jeopardizing the computing times. The advantage of the use of such advanced structural models mainly lies in their modeling flexibility, thus greatly reducing the (re-)modeling effort after small changes to the system 1. In comprehensive rotor codes the modal reduction approach is used, which requires new software developments for each new mechanical model, see for instance Kunz and Jones 11, who modify CAMRAD to model the intricate Apache rotor system.



Advanced aerodynamics rotor codes can be used to supplement the rotor codes at level A or B, and improve their applicability by using the results as linearization point.

Current helicopter codes which apply Euler/Navier-Stokes models for the aerodynamics use structural dynamics models at level 1 (Wagner et al.25), or apply only weak coupling between the aerodynamics and the structural dynamics (Servera et al.18, Pahlke et al.16).

1.3 Towards advanced rotor codes

For the quantitative resolution of the aeroelastic response problem of a rotor/hub/fuselage system resulting in vibrations, it is required that an accurate aerodynamics model is coupled with a detailed elastomechanical model.

Compared to monodisciplinary simulations, computing times for the coupled simulation increase significantly, because of the disparate time scales of the problem. For helicopter simulations, the ratio of the maximum frequency of the flow physics, the BVI events, and the minimum frequency, the blade passing frequency, is in the order of hundreds. The structural dynamics reacts on the same time scale as the BVI events, whereas a trimmed solution can only be verified after the simulation of a complete revolution. Hence, a simulation of a trimmed rotor configuration including blade deformation takes a large number of revolutions.

The large number of revolutions required for coupled simulations has prompted the development of so-called weakly coupled aeroelastic simulations, where the elastomechanical model and trimming procedure are computed using standard comprehensive rotor codes based on mixed potential and lifting line models. The forces from the relatively simple aerodynamics of the rotor codes are corrected by the Computational Fluid Dynamics (CFD) results, and the blade pitch and blade deformations from the rotor code are passed to the CFD grid system. See Pahlke et al. 16 and Servera et al. 18 for an overview of this method. Since the rotor trim and blade deformations still depend on two-dimensional aerodynamical models, this will result in a degradation of the accuracy compared to using the 3D CFD data directly. For instance, Boelens et al. 3 found that it is essential to trim the rotor based on the CFD results, and not on the aerodynamic models used in comprehensive rotor codes. Hence, a *strong* coupling of the elastomechanical model and trim procedure with the CFD results is preferred, where the different models interact directly.

Combination of the accuracy requirements with the system requirements of the coupled models shows that it is of the utmost importance that the computing times of the computationally most intensive part, the aerodynamic computations, are reduced significantly. This is the subject of the current report. A solution algorithm, of which the first ideas were introduced in Van der Ven et



al. 24, will be demonstrated for the simulation of a trimmed rotor in forward flight with deforming blades.

1.4 Outline

The outline of the paper is as follows. In the next section the solution algorithm is described. In Chapter 3 the simulation of a BO105 rotor system in forward flight is described in detail, and the computational complexity of the simulation is examined. Finally, conclusions are drawn.



2 Multitime multigrid algorithm

In this section the multitime multigrid (MTMG) algorithm of Van der Ven et al. 24 for solving time-periodic problems is described and its application to rotor flow is discussed.

2.1 Basic idea

The basic idea of the MTMG solution algorithm is that a time-periodic problem can be considered a steady problem in the sense that after one time period the next period shows the same flow phenomena, as exposed in more detail in Van der Ven et al. 23, 24. This is formalised by solving the time-dependent flow equations simultaneously in both space and time for the complete period of the problem. This is contrary to the usual time-serial approach, where one proceeds time step after time step on spatial grids. Now the time-dependent equations are solved on a four-dimensional space-time grid which contains all time levels in a period.

The solution approach of the four-dimensional equations is the same as for three-dimensional equations: a pseudo-time is introduced and the solution is marched to steady-state in pseudo-time by a four-dimensional multigrid algorithm. This approach is feasible since the time-dependent compressible Euler equations are hyperbolic in both space and time, hence the temporal direction can be treated like the spatial directions.

It is important to realise that the proposed algorithm is a convergence acceleration algorithm for time-dependent equations. The discretization scheme is not modified, hence its accuracy properties are retained.

2.2 Benefits

Apart from generating a periodic solution by construction, the main advantage of the solution algorithm lies in the fact that it transforms a time-dependent (*dynamic*) problem into a steady-state (*static*) problem. This has several advantages:

- as long as the solution process converges, the final solution is independent of the solution process. The underlying discretised equations are unmodified, and, moreover, there is no problem with the possible accumulation of numerical errors from preceding time steps;
- local grid refinement can be extended to the time dimension. Since there is no time direction in the solution algorithm, interpolation or the order of time steps in the case of hanging nodes are no issue;
- combining local grid refinement and parallel processing does not lead to dynamic load balancing problems. Since the local grid refinement no longer needs to be applied at each time step, the number of grid adaptations reduces significantly to about five times per simulation,

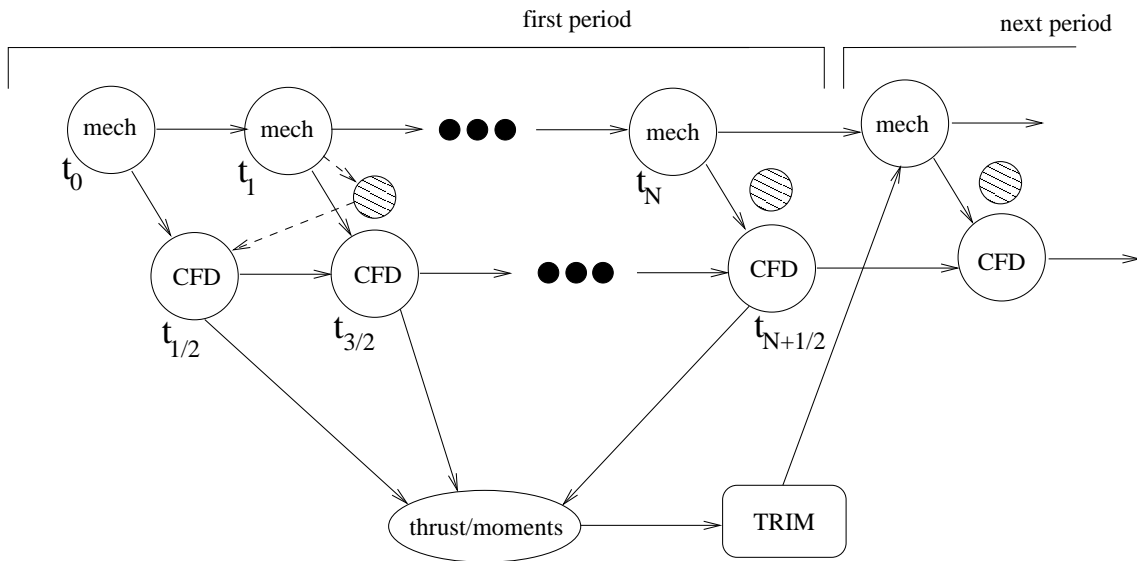


Fig. 1 Conventional time serial coupling procedure for the aeroelastic modeling of the rotor/hub/fuselage system, including trim. Shown is the implicit/implicit staggered scheme of Wagner et al. 25. After each revolution the thrust and moments are collected and used to trim the rotor system, after which the mechanics/CFD iterations are restarted.

which is the usual number for steady-state simulations. Hence the parallel efficiency on a massively parallel processors machine is not hindered by dynamic load balancing issues. Because of the grid sizes of four-dimensional grids it is expected that the MTMG algorithm easily scales to thousands of processors;

- time-accurate coupling with other physics models is straightforward.

For the strongly coupled aeroelastic simulation of a trimmed rotor/hub/fuselage system all these benefits help to decrease the computational complexity of the simulation.

Conventionally, the solution procedure for the aeroelastic simulation is as shown in Figure 1, based on the implicit/implicit staggered scheme of Wagner et al. 25 and Piperno et al. 17. After each period, the thrust and moments can be computed and used to trim the rotor, after which a new period is simulated. If grid adaptation were applied, dynamic load balancing problems would occur, effectively destroying any existing efficiency in other parts of the aerodynamics model than the adaptation algorithm.

In the MTMG approach all simulation data is available at all time steps, and the trust and moments are readily available to trim the rotor. Moreover, a modification in the pitch schedule will require only a small number of pseudo-time iterations for the flow solution to conform to the new schedule. Another consequence of having the data available at all time steps is that the coupling between

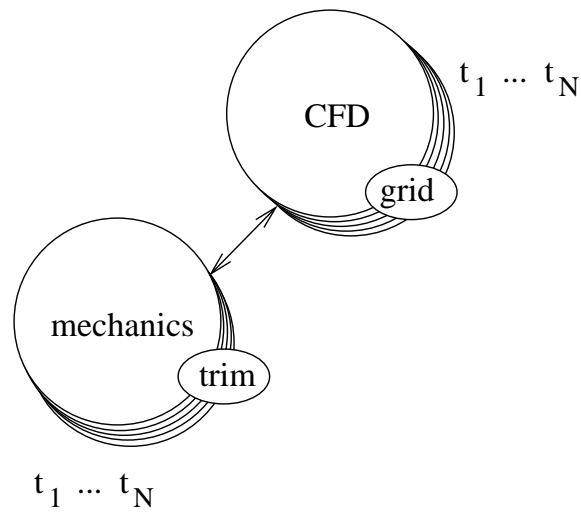


Fig. 2 Coupling procedure for the aeroelastic modeling of the rotor/hub/fuselage system, including trim and grid adaptation, using the MTMG solution algorithm.

the aerodynamics and mechanics modules can be made genuinely implicit, without the need of predictor-corrector mechanisms.

Since local grid refinement will not lead to dynamic load balancing issues in the MTMG approach, local grid refinement can be applied to decrease the required grid size. The coupling procedure for the aeroelastic simulation using the MTMG approach, including trim and grid adaptation, is shown in Figure 2.

3 Rotorcraft simulation

In the absence of experimental data, the current report focuses on the feasibility of the coupling strategy. It will be investigated how the trim procedure of 2 interacts with the aerostructural coupling and what the computational requirements are to obtain a trimmed rotor system with deforming blades. The algorithm will be applied to the four-bladed BO105 rotor.

3.1 Structural model

To allow blade deformations due to aerodynamic forces a one-dimensional linear beam model is used to describe blade deformation through coupled bending and torsion. As described in the introduction this is a structural model at sophistication level 1, which is sufficient to demonstrate the feasibility of the current framework.

The equations for bending and torsion of the beam are obtained from linear beam theory, and are described in the book by Johnson 10 and the review article by Kunz 12. Lead-lag deformations are neglected since the current aerodynamic model is not able to predict the drag due to viscous effects. For the same reason, the blade twist is only modeled as an addition to the pitch schedule, and its effect on the lead-lag deformation (which would require more material properties) is neglected. Moreover it is assumed that both the pitch axis and the elastic axis intersect with the hub center, and that the flap hinge offset is zero. As a last assumption, the blade flapwise radius of gyration is assumed to be much larger than the blade chordwise radius of gyration.

At the root the Dirichlet boundary conditions $w = 0$, $\frac{\partial w}{\partial \xi} = 0$, and $\theta = 0$ are applied. That is, we assume that the pitch schedule is enforced at the root. More realistically, we could have modelled the control system's restoring moment, but the Dirichlet boundary condition is assumed to be sufficient for the moment.

Material properties of the BO105 blade are obtained from the Wind Tunnel Model Database of the Helinovi project 5. In this database the material properties are presented as needed by the comprehensive rotor code CAMRAD/JA. The eigenfrequencies of the *nonrotating* beam have been validated by the experimental eigenfrequencies. The eigenfrequencies of the rotating beam, as modeled in CAMRAD/JA, are presented in Table 3, together with the eigenfrequencies of the beam model.

The beam model models both the aerodynamic blade and the blade between the hinges and the root cut-out. Hence the beam's origin lies at $r/R = 0.075$, and the beam's tip at $r/R = 1$. Aerodynamic forces are computed from the root cut-out at $r/R = 0.22$ up to the tip at $r/R = 1$. There are 8 non-uniformly distributed beam elements between the hinges and root cut-out, and 28 uniformly distributed elements between the root cut-out and the tip.



Table 3 Eigenfrequencies (per revolution) of the BO105 beam models of CAMRAD/JA (5) and the linear beam model

	CAMRAD/JA	type	Beam model
1	0.815	lag	-
2	1.144	flap	1.11
3	2.872	flap	2.87
4	3.577	torsion	3.77
5	5.073	flap	4.96
6	5.315	lag	-
7	8.064	flap	7.54
8	10.517	torsion	10.67

3.2 Aerodynamic model

Between the root cut-out at $r/R = 0.22$ and the tip the BO105 blade has a rectangular platform and a cross-sectional geometry defined by the NACA23012 airfoil with modified trailing edge. The real blade has a 5mm long tab with a width of 0.9 mm attached to the trailing edge. In the aerodynamic model the tab end is closed, but otherwise present. The blade has a linear twist of -8 degrees. The root and tip of the aerodynamic blade are rounded off. The taper between $r/R = 0.175$ and $r/R = 0.22$ is not modeled.

The compressible Euler equations of gas dynamics are solved using the discontinuous Galerkin finite element method in an arbitrary Lagrangian-Eulerian formulation to accommodate moving meshes. Details of the flow solver can be found in Van der Vegt et al.22.

All computations are performed on a four dimensional mesh containing the full time period of a quarter revolution (since the BO105 rotor has four blades). The spatial part of the mesh, containing the four blades in a single boundary conforming mesh, originally consists of 377,000 cells. The number of time steps is 20 (that is, 4.5 degrees azimuthal angle), so the four-dimensional mesh consists of 7,500,000 cells, corresponding to about 200 million degrees of freedom.

3.3 Flight conditions

The tip Mach number is 0.641, and the advance ratio is 0.195 (freestream Mach number of 0.125). The rotor plane is tilted over -0.66 degrees. Precone angle is 2.5 degrees. The thrust is 0.0044. Based on a medium mesh computation the rotor system with deforming blades has been trimmed, leading to a pitch schedule defined by

$$\theta_{\text{con}} = 5.64^\circ + 2.15^\circ \cos \psi - 2.15^\circ \sin \psi, \quad (1)$$


```

while not trimmed do
  while blade motions change do
    decrease flow residuals
    compute elastic blade motion
  endwhile
  compute new pitch schedule
endwhile

```

Fig. 3 Trimming procedure for MTMG simulation of rotor with deforming blades

where ψ is the azimuth angle measured from the tail rotor. The flap schedule is zero. The above pitch schedule is the starting point for the fine grid simulation, and will be modified by the trimming process.

3.4 Trim

Both the blade deformation and the trim procedure are iterative procedures. This means that there are several choices on how to combine the two iterative loops. In the following simulations the trim loop is the outer loop, and the deformation is the inner loop (see Figure 3). The trim procedure requires a sensitivity matrix of the aerodynamic forces with respect to the collective, lateral, and longitudinal pitch settings. The sensitivity matrix includes the effects of the blade deformation on the aerodynamic forces.

The sensitivity matrix has been computed on one time coarsened mesh and at the point $(\theta_0, \theta_{1c}, \theta_{1s}) = (5.64, 2.15, -2.15)$ is found to be:

$$\begin{pmatrix} \frac{\partial C_T}{\partial \theta_0} & \frac{\partial C_T}{\partial \theta_{1c}} & \frac{\partial C_T}{\partial \theta_{1s}} \\ \frac{\partial C_{M_x}}{\partial \theta_0} & \frac{\partial C_{M_x}}{\partial \theta_{1c}} & \frac{\partial C_{M_x}}{\partial \theta_{1s}} \\ \frac{\partial C_{M_y}}{\partial \theta_0} & \frac{\partial C_{M_y}}{\partial \theta_{1c}} & \frac{\partial C_{M_y}}{\partial \theta_{1s}} \end{pmatrix} \approx 10^{-4} \begin{pmatrix} 4.3 & 0.1 & 0.7 \\ 0.2 & 0.8 & 0.7 \\ 0.3 & -1.3 & 1.0 \end{pmatrix}.$$

Throughout the simulation it is assumed that the trimming matrix is constant, since recomputing the matrix at other linearization points is costly, and the expectation is that it is sufficient for finding a trimmed solution.

3.5 Grid adaptation

The grid adaptation is designed to improve the vortex resolution in the CFD simulation. The refinement is based on a vortex sensor combined with a mesh width or time step sensor. Whenever a cell has a vorticity level higher than a specified level *and* the mesh width in a certain direction

is greater than a specified resolution length, the cell is refined in that direction. In the temporal direction a cell is refined when the physical CFL number is greater than two within a vortex. The spatial resolution length is $R/200$, where R is the rotor radius (see 3, 23 for a more detailed discussion on grid quality for the simulation of rotor flows).

3.6 Simulation strategy

The trim, blade deformation, and grid adaptation algorithms each change the represented flow phenomena (either by a change of the blade motion, or more resolved tip vortices), and hence the particular sequence in which the algorithms are applied has important consequences on the simulation results and/or computational efficiency. The grid adaptation algorithm is used to increase vortex resolution in order to detect blade-vortex interactions. The blade-vortex interactions constitute a higher-order harmonic effect than the trim of the rotor system. Therefore the chosen simulation strategy is first to trim the system of deforming blades using the original aerodynamic mesh, and then to locally refine the mesh to increase vortex resolution. After the grid adaptation, the rotor system is trimmed again, which should have only local effect on the blade motions. Whether this assumption is correct, will be investigated.

3.7 Results

3.7.1 Trim

The trim procedure as described in Figure 3 is executed. A (part of a) typical convergence history of the flow residuals is shown in Figure 4. Each spike in the convergence history signifies a change in the mesh, either caused by the grid sequencing algorithm at the start of the simulation, the blade deformation algorithm, or a change of pitch schedule. The complete trim procedure required three changes of pitch schedule, and a total of fourteen elastic blade deformations. The convergence history of the change in elastic pitch is shown in Figure 5. The coupling with the aerodynamic model is relaxed to improve convergence, with underrelaxation 0.25.

The trimmed pitch schedule is $\theta_{\text{con}} = 7.9^\circ + 2.0^\circ \cos \psi - 2.4^\circ \sin \psi$, which, apart from the collective, is quite close to the original pitch schedule (1). During the trim procedure, however, lateral and longitudinal pitch changed significantly before returning close to their original values. That the search path is not optimal may suggest that the sensitivity matrix is not sufficiently accurate.

The elastic blade motion of the trimmed rotor system is shown in Figure 6.

3.7.2 Temporal adaptation

In order to obtain the blade loads with increased temporal resolution, the grid adaptation started with grid refinements in time only. The temporal resolution is increased from 4.5° azimuth to

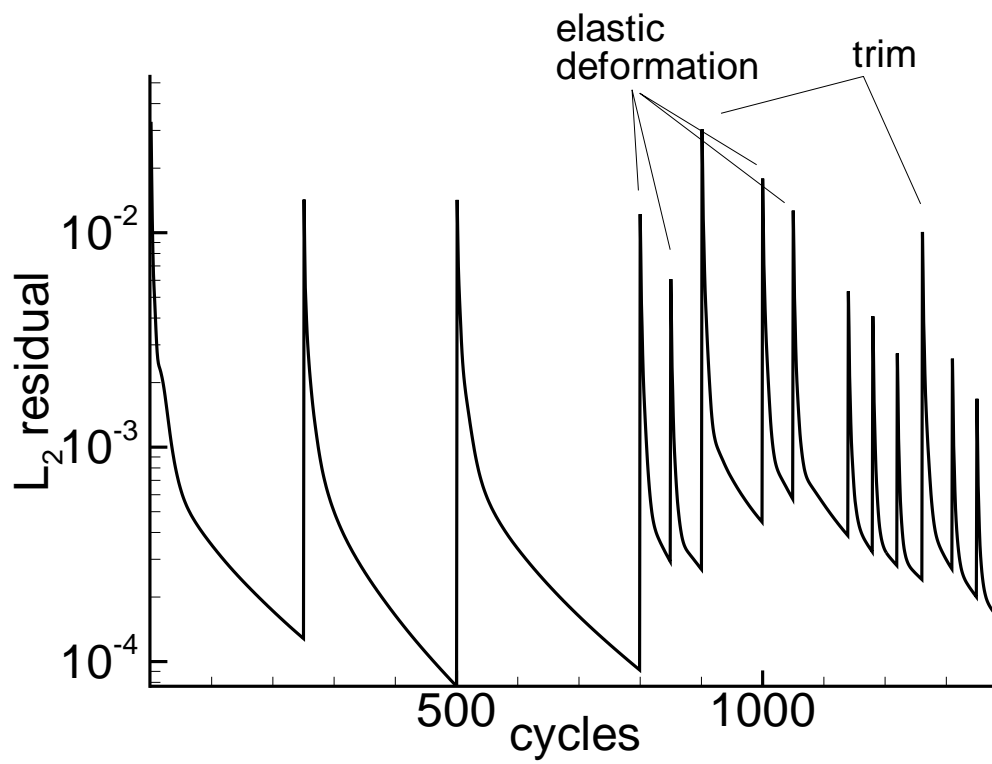


Fig. 4 Part of the convergence history of the flow residuals of the simulation showing the grid sequencing, blade deformation, and trim processes

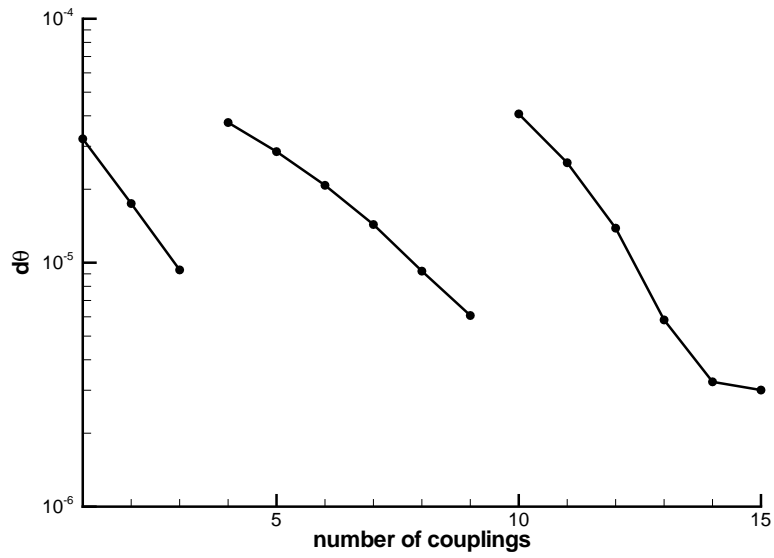


Fig. 5 The convergence history of the elastic pitch in the trimming procedure. Three changes of pitch schedule are shown.

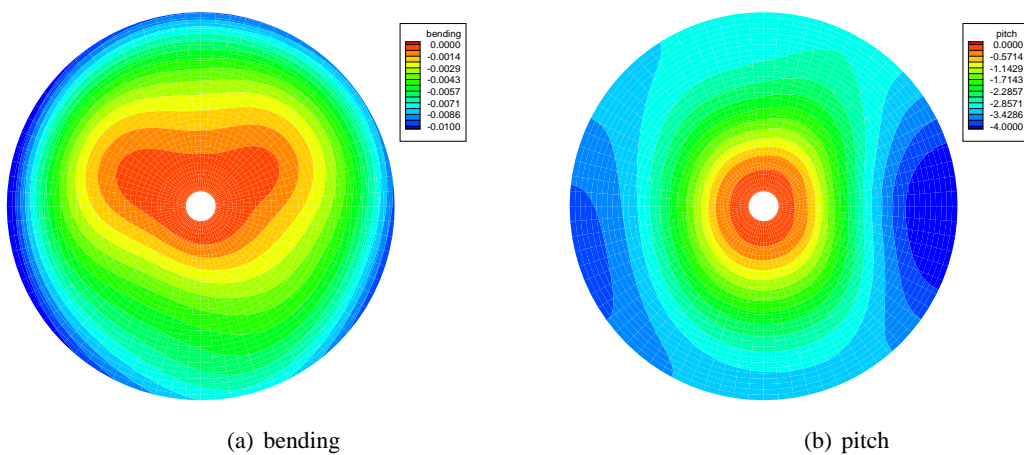


Fig. 6 The elastic bending and pitch of the trimmed rotor system on the original mesh.

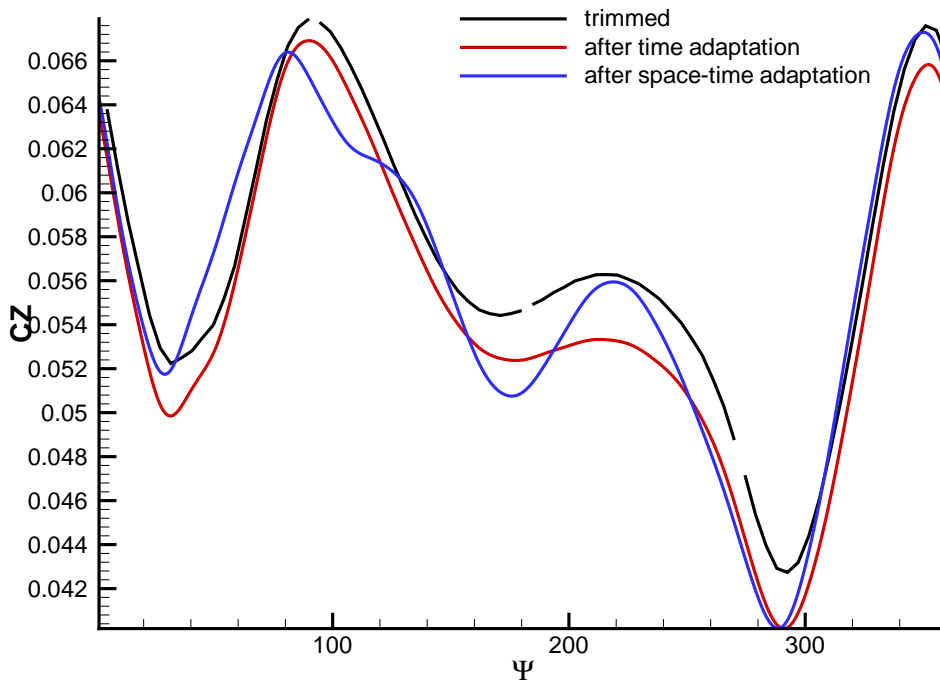


Fig. 7 The blade thrust coefficient on the original mesh (black line), after temporal adaptation (red line), and after space-time adaptation (blue line).

1.125° azimuth. The adaptation algorithm is implemented in such a way that the complete blade representation is present at all (new) time levels. Hence the blade loads can be determined for all time levels. It should be noted, however, that the spatial grids at the newly created, intermediate, time levels do not cover the complete domain. The adapted mesh, with a factor four increase of temporal resolution near the blades, contains 9 million elements, an increase of only 20%. A comparison of the blade loads (in terms of blade thrust coefficient) before and after the adaptation is shown in Figure 7. The signal is significantly smoother, but otherwise not much affected.

3.7.3 Space-time adaptation

After the temporal adaptations, the grid is refined in space and time simultaneously. The time refinement is such that the smallest azimuth angle remains 1.125°. Two spatial sensor levels are applied to test their effectiveness. First, the vorticity level above which a cell may be refined is $0.75a_\infty/R$, where a_∞ is the freestream speed of sound. Second, this level is increased to $2a_\infty/R$. It is found that the first vorticity threshold leads to excessive refinement in the vortex sheet, while the second vorticity threshold mainly refines within the vortex core, which is the most beneficial

for increased vortex persistence.

The final refined mesh contains 19 million grid cells, which corresponds to 475 million degrees of freedom.

An example of the effect of local grid refinement is shown in Figure 8. The increase in vortex strength and persistence can be clearly seen, especially for the retreating blades. The grid resolution within the vortex is examined in Figure 9. Clearly, the numerical method is able to obtain excellent flow results on highly irregular grids. The resolution within the vortex core is about six cells in each direction.

3.7.4 Final trim

After the grid refinements the rotor system is no longer trimmed, since the improved time resolution and vortex signature change the loads on the blades. So the rotor system is trimmed once more. The trimmed pitch schedule is $\theta_{\text{con}} = 7.9^\circ + 1.5^\circ \cos \psi - 2.4^\circ \sin \psi$, which is, as expected, quite close to the trimmed pitch schedule on the original mesh. Results are shown in Figure 10 up to 12. Figure 10 compares the sectional lift and moment distributions over the rotor disk of the trimmed solution on the original grid and the final refined mesh. Clearly, the enhanced time resolution improves the smoothness of the forces, and especially the sectional moment distribution is changed significantly. However, there are no distinct blade-vortex interactions.

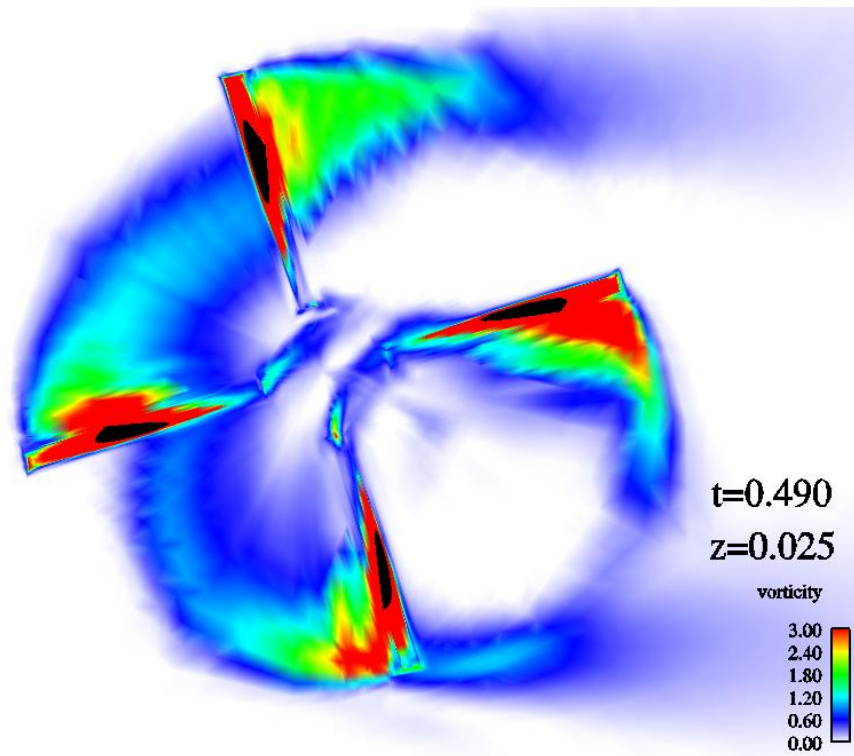
More detail is shown in Figures 11 and 12, which show the sectional lift and moment at two radial stations. The lift and moment distribution on the final mesh display more oscillatory detail, especially for the advancing blade. Hence, the local grid refinement improves the oscillatory detail in the external loads, which is essential for accurate prediction of vibratory loads.

3.8 Computational complexity

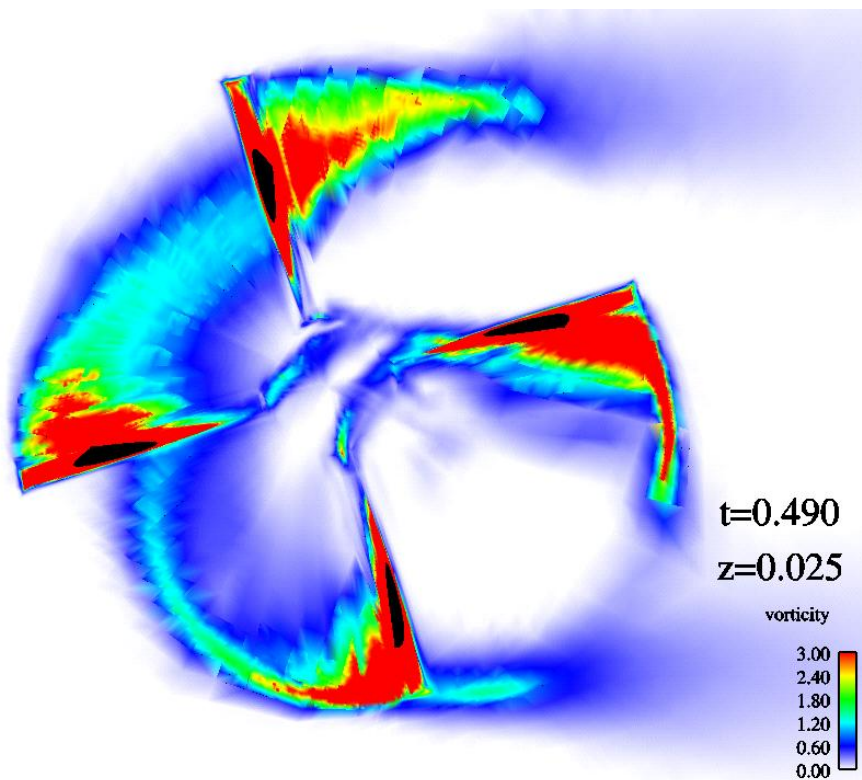
A detailed analysis of the computational complexity of the current algorithm, compared with the conventional approach, has been presented in 23. Summarizing from 23 there are two sources of the significant reduction of computing time:

- The ratio of the number of periods required to obtain a periodic, elastically trimmed, solution in the conventional time serial algorithm and the number of CFD grid modifications in the current algorithm (due to trim, elastic deformation, and grid refinement).
- The grid size ratio of the two algorithms.

The above described simulation requires three rotor trims, each requiring about four elastic deformations, and ten grid adaptations to achieve the required resolution. The number of periods

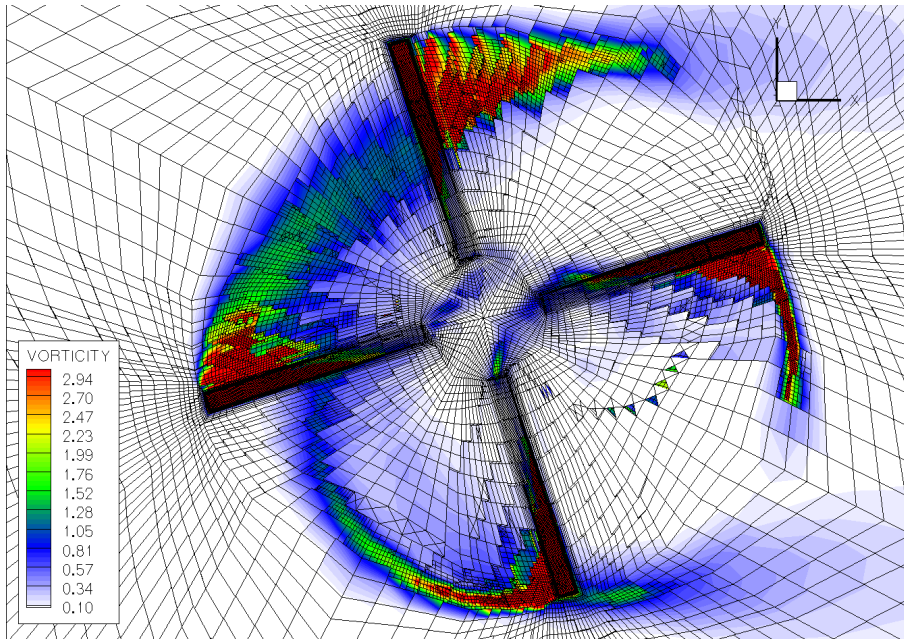


(a) original mesh

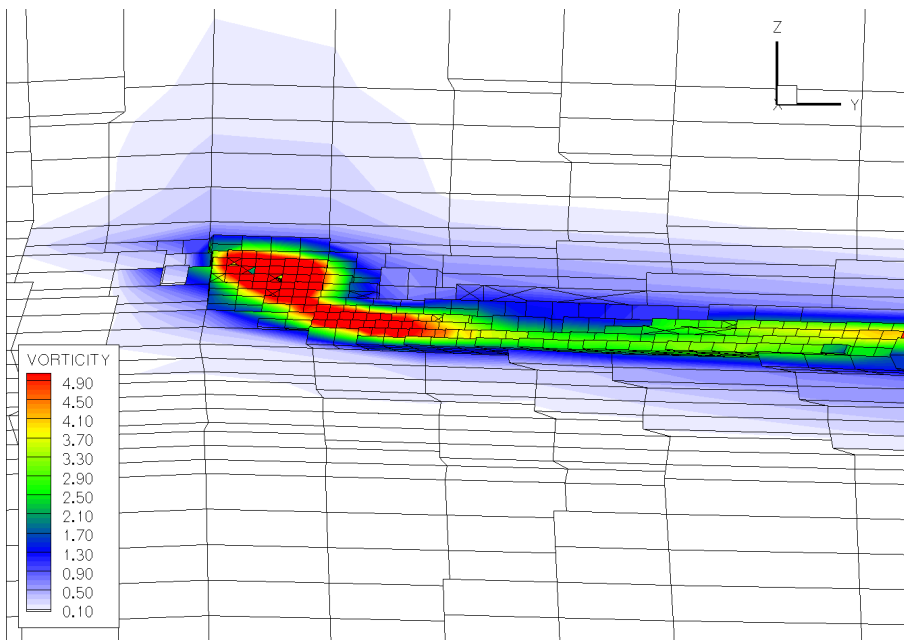


(b) adapted mesh

Fig. 8 Vortex resolution in a horizontal cross-plane for the original mesh (top), and the final adapted mesh (bottom). Flow is coming from the left.



(a) horizontal plane



(b) vertical plane

Fig. 9 Grid resolution in a horizontal cross-plane (top) and a vertical plane (bottom) for the final adapted mesh.

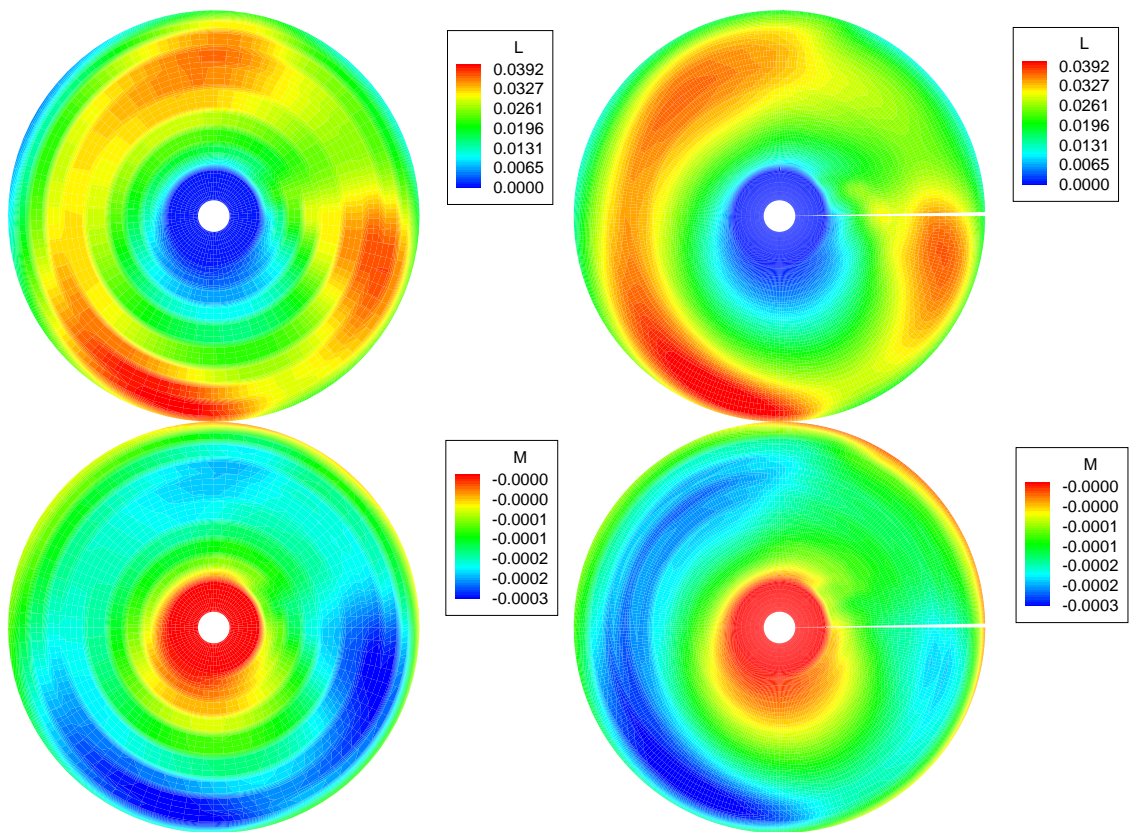


Fig. 10 The sectional lift and moment coefficient distribution over the rotor disk for the unadapted original mesh and the final refined mesh

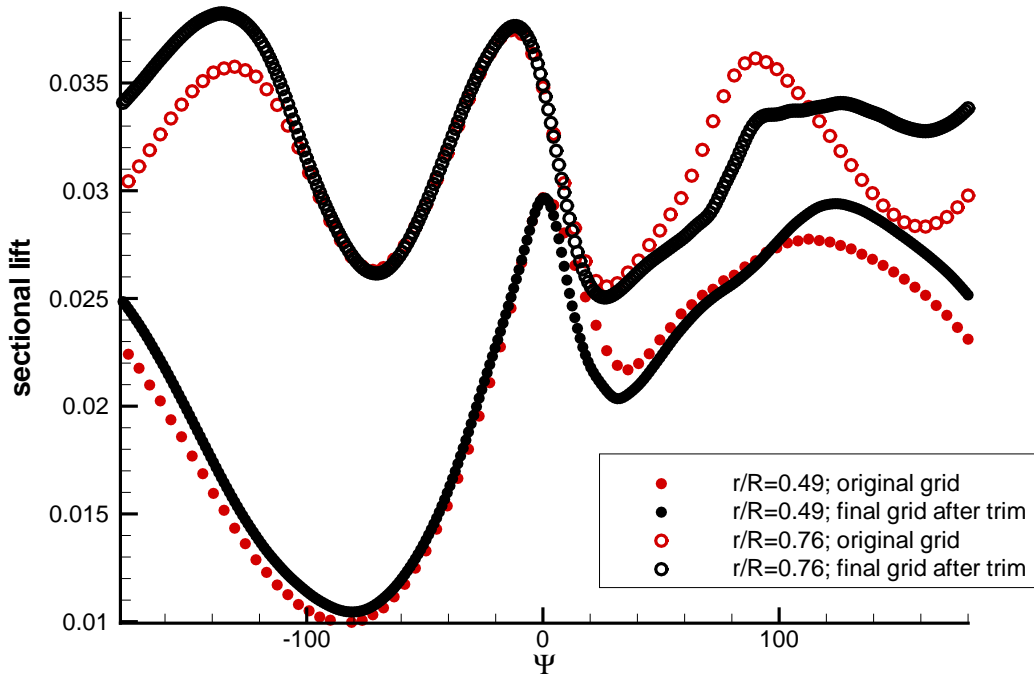


Fig. 11 The sectional lift coefficient distribution for two radial stations for the unadapted original mesh and the final refined mesh. Red: original mesh; black: final mesh. Closed circles: $r/R = 0.76$; open circles: $r/R=0.49$.

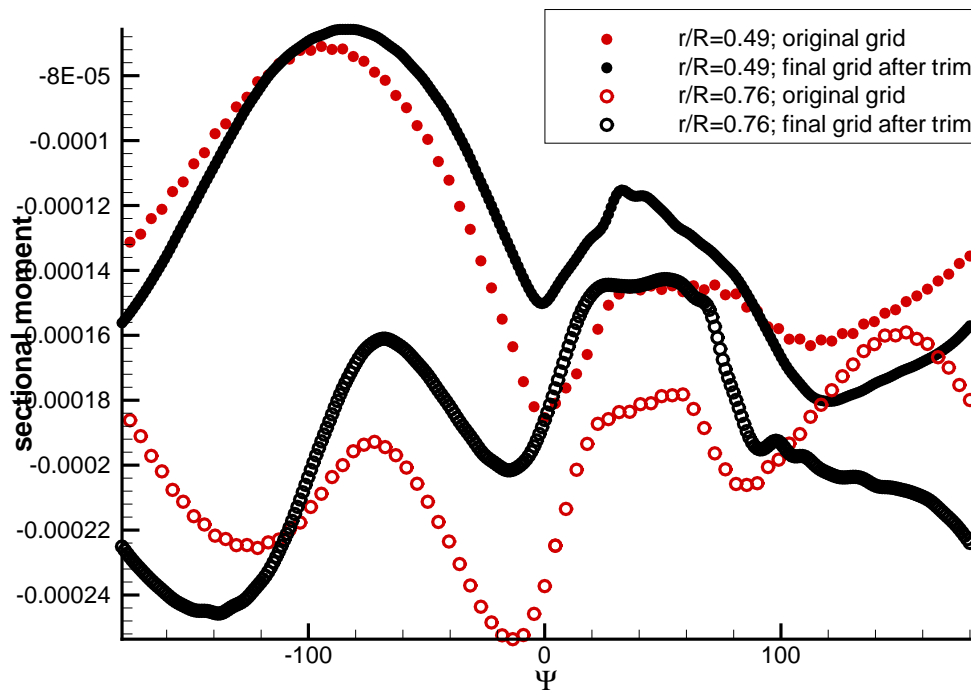


Fig. 12 The sectional moment coefficient distribution for two radial stations for the unadapted original mesh and the final refined mesh. Red: original mesh; black: final mesh. Closed circles: $r/R = 0.76$; open circles: $r/R=0.49$.



required to obtain a periodic and elastically trimmed solution using the conventional time-serial algorithm is difficult to estimate, but, considering the results in 24, convergence to a periodic solution is extremely slow, let alone the convergence rate to an elastically trimmed solution. An estimated number of one hundred periods is not overly conservative (Wagner et al. 25 use 64 periods for a trimmed aeroelastic simulation and are not satisfied with the periodicity of the solution). Hence the ratio of the number of periods and grid modifications and periods is $100/22 \approx 5$.

Based on the required grid resolution in the vortex, the theoretical ratio of grid sizes is estimated as 64 in 23. The current simulation requires 19 million cells, whereas the (space-time) grid size in 3 for the simulation of the vortex flow about an Operational Loads Survey rotor is reported as 188 million; a ratio of 10. The fact that the theoretical ratio has not been achieved, is caused by the excessive refinement in the vortex sheet. The size of the vortex sheet is roughly the size of the rotor disk, and scales as an area, quadratically with rotor radius, whereas the tip vortex region scales linearly.

Combining the speedup ratio's, the overall speedup of the current algorithm with respect to the conventional algorithm is 50.

The current simulation has been executed on six processors of the NEC SX-5B vector processor. The flow solver has a sustained performance of 18 Gflop/s on the six processors, and the complete simulation including the three trims and the ten grid adaptations requires 50 wall-clock hours. Considering the fact that current supercomputers are at least ten times faster than the computer used, and the inherent scalability of the solution algorithm, this wall-clock time can be reduced to five hours on a modern supercomputer.

4 Conclusions

The level of external vibratory loads is important for many operational aspects of helicopters. For the prediction of these vibratory loads near the border of the flight envelope a predictive tool based on first-principles physics is studied.

Straightforward application of existing algorithms for structural dynamics, aerodynamics, and flight control, based on a first-principles physical description, would yield a helicopter vibration analysis framework which requires prohibitively large computing times, due to disparate time scales and high resolution requirements. To overcome the apparent computational complexity of the system, a fourdimensional solution method has been presented. The solution method decreases both the numerical complexity of the coupled system, and its computational complexity, by turning a dynamic problem into a static problem. Local grid refinement can be used to decrease the aerodynamic grid size, without jeopardising the parallel efficiency of the method.

The solution method has been successfully applied to the trimmed, aeroelastic, simulation of the flow around a rotor in forward flight, with local grid refinement for increased vortex persistence.

The computational complexity of the most compute-intensive part of the coupled system for aeroelastic response problems has been reduced significantly. A clear development path has been identified to reach the ultimate goal of affordable and accurate vibrational analysis of rotor/hub/fuselage systems.

Future work will include experimental validation and increase of the sophistication level of the structural dynamics of the rotor system.

Acknowledgement

The support of R.J.J. Bakker, J. van Muijden, and N. Munninghof (NLR) is gratefully acknowledged.



5 References

1. O.A. Bauchau, C.L. Bottasso, and Y.G. Nikishkov. Modeling rotorcraft dynamics with finite element multibody procedures. *Math. Comput. Modeling*, 33:1113–1137, 2001.
2. O.J. Boelens, H. van der Ven, B. Oskam, and A. Hassan. Accurate and efficient vortex-capturing for rotor blade-vortex interaction. *AIAA*, 2000-0112, 2000.
3. O.J. Boelens, H. van der Ven, B. Oskam, and A.A. Hassan. Boundary conforming discontinuous Galerkin finite element approach for rotorcraft simulations. *J. of Aircraft*, 39 (5):776–785, sep-oct 2002.
4. C.L. Burley, T.F. Brooks, B.D. Charles, and M. McCluer. Tiltrotor aeroacoustic code (TRAC) prediction assessment and initial comparison with TRAM test data. In *Proceedings of the 25th European Rotorcraft Forum, September 14-16, 1999, Rome*, 1999.
5. O. Dieterich. Wind tunnel model database. Technical Report HeliNOVI D 2.1-1, version 1.0, ECD, 2002.
6. P. Wilders et al., editor. *International Parallel CFD 2001 Conference*. North-Holland, Elsevier, May 21-23 2002.
7. P.H. Gander, R.M. Barnes, K.B. Gregory, L.J. Connell, D.L. Miller, and R.C. Graber. Crew factors in flight operations VI: Psychophysiological responses to helicopter operations. Technical Report TM 108838, NASA Ames Research Center, 1994.
8. D.J. Haas and C.G. Schaefer, Jr. Emerging technologies for rotor system health monitoring. In *52nd American Helicopter Society Forum, Washington D.C., June, 1996*, 1996.
9. M.H.L. Hounjet, J.C. Balleur, D. Blaise, G. Bernardini, and A. Pisoni. Maturation of a full potential based rotor flow field code. In *Proceedings of the 26th European Rotorcraft Forum, The Hague, The Netherlands, September 26-29, 2000*, 2000.
10. Wayne Johnson. *Helicopter Theory*. Princeton University Press, Princeton, New Jersey, 1980.
11. H.E. Jones and D.L. Kunz. Comprehensive modeling of the Apache with CAMRAD II. In *Proceedings of the American Helicopter Society Hampton Roads Chapter, Structure Specialists' Meeting, Williamsburg, October 30-November 1, 2001*, 2001.
12. Donald L. Kunz. Survey and comparison of engineering beam theories for helicopter rotor blades. *J. of Aircraft*, 31 No. 3, 1994.
13. K.H. Lyle, C.L. Burley, and D.S. Prichard. A comparison of measured and predicted XV-15 tiltrotor surface acoustic pressures. In *Proceedings of the AHS Technical Specialists' Meeting for Rotorcraft Acoustics and Aerodynamics, October 28-30, 1997, Williamsburg*, 1997.
14. Kelly McCool and Gene Barndt. Assessment of helicopter structural usage monitoring system requirements. Technical Report ASW-112, US Department of Transportation, April 2004.

15. J. Milgram and I. Chopra. Helicopter vibration reduction with trailing edge flaps. In *Proceedings of the 36th AIAA/ASME/ASCE/AHS/ASC Structures, Structural Dynamics, and Material Conference, April 10-12, 1995, New Orleans, 1995*.
16. K. Pahlke and B. van der Wall. Progress in weak fluid-structure-coupling for multibladed rotors in high speed forward flight. In *Proceedings of the 28th European Rotorcraft Forum, September 17-20, 2002, Bristol, 2002*.
17. S. Piperno, C. Farhat, and B. Larrouturou. Partitioned procedures for the transient solution of coupled aeroelastic problems, Part I: Model problem, theory and two-dimensional application. *Comput. Meth. Appl. Mech. Engrg.*, 24:79–112, 1995.
18. G. Servera, P. Beaumier, and M. Costes. A weak coupling method between the dynamics code HOST and the 3D unsteady Euler code WAVES. In *Proceedings of the 26th European Rotorcraft Forum, September 26-29, 2000, The Hague, 2000*.
19. Patricia W. Stevens, David L. Hall, and Edward C. Smith. A multidisciplinary approach to rotorcraft health and usage monitoring. In *52nd American Helicopter Society Forum, Washington D.C., June, 1996*, pages 1732–1751, 1996.
20. I.Y. Tumer and A. Bajwa. A survey of aircraft engine health monitoring systems. In *The 1999 Joint Propulsion Conference, Los Angeles, CA. June 1999, 1999*.
21. I.Y. Tumer and R.B. Stone. Analysis of triaxial vibration data for health monitoring of helicopter gearboxes. *ASME Journal of Vibration and Acoustics*, 125:120–128, 2003.
22. J.J.W. van der Vegt and H. van der Ven. Space-time discontinuous Galerkin finite element method with dynamic grid motion for inviscid compressible flows. Part I. General formulation. *J. Comput. Phys.*, 182:546–585, 2002.
23. H. van der Ven and O.J. Boelens. Towards affordable CFD simulations of rotor in forward flight – a feasibility study with future application to vibrational analysis. In *proceedings of the 59th American Helicopter Society Forum, Phoenix, Arizona, USA, May 6-8, 2003, 2003*.
24. H. van der Ven, O.J. Boelens, and B. Oskam. Multitime multigrid convergence acceleration for periodic problems with future applications to rotor simulations. In 6, pages 355–363, 2002.
25. S. Wagner, A.R.M. Altmikus, and H. Pomin. Coupled numerical simulation of aerodynamics and rotor dynamics of a helicopter in forward flight. In *Proceedings of the Fifth World Congress on Computational Mechanics, Vienna, Austria, July 7th - 12th, 2002*, <http://wccm.tuwien.ac.at/>, 2002.
26. H. Yeo and P.M. Shinoda. Investigation of rotor loads and vibration at transition speed. In *Proceedings of the American Helicopter Society 58th Annual Forum, June 11-13, 2002, Montreal, 2002*.